NASA Technical Memorandum 89080

HIGHLIGHTS OF UNSTEADY PRESSURE TESTS ON A 14 PERCENT SUPERCRITICAL AIRFOIL AT HIGH REYNOLDS NUMBER, TRANSONIC CONDITION

ROBERT W. HESS, DAVID A. SEIDEL,
WILLIAM B. IGOE, AND PIERCE L. LAWING

JANUARY 1987

Corrected Copy

National Aeronautics and Space Administration

Langley Research Center
Hampton, Virginia 23665

HIGHLIGHTS OF UNSTEADY PRESSURE TESTS ON A 14 PERCENT SUPERCRITICAL AIRFOIL AT HIGH REYNOLDS NUMBER, TRANSONIC CONDITION

Robert W. Hess*, David A. Seidel**, William B. Igoe***,
and Pierce L. Lawing****
NASA Langley Research Center
Hampton, Virginia 23665-5225

Abstract

Steady and unsteady pressures were measured on a 2-D supercritical airfoil in the Langley Research Center 0.3-m Transonic Cryogenic Tunnel at Reynolds numbers from 6 x 10^6 to 35 x 10^6. The airfoil was oscillated in pitch at amplitudes from ±.25 degrees to ±1.0 degrees at frequencies from 5 Hz to 60 Hz. The special requirements of testing an unsteady pressure model in a pressurized cryogenic tunnel are discussed. Selected steady measured data are presented and are compared with GRUMFOIL calculations at Reynolds number of 6 x 10^6 and 30 x 10^6. Experimental unsteady results at Reynolds numbers of 6 x 10^6 and 30 x 10^6 are examined for Reynolds number effects. Measured unsteady results at two mean angles of attack at a Reynolds number of 30 x 10^6 are also examined.

Nomenclature

c	chord
C_l	lift coefficient
C_p	pressure coefficient
$\lvert C_p \rvert$	modulus of oscillating pressure coefficient
f	frequency, Hz
k	reduced frequency, based on semichord, $\pi cf/V$
M	Mach number
P_1, P_2	Pressures in flow restrictor calibration, figure 5
R	Reynolds number based on chord
V	velocity, ft/sec
x	streamwise coordinate measured from leading edge, in.
α	peak oscillation amplitude in pitch, degrees, positive leading edge up, deg.
$\bar{\alpha}$	steady or mean dynamic amplitude in pitch, positive leading edge up, deg.
μ	micron, 1 x 10^{-6} meters
ϕ	phase angle between oscillating pressure and oscillating wing pitch angle, deg.

Subscripts

c	corrected value
t	test measurement

Introduction

The advent of large cryogenic wind tunnels allows unsteady pressure measurements to be made on models at Reynolds numbers typically experienced by high performance aircraft, thus eliminating the need for artifices such as boundary-layer trips to simulate boundary layer transition at high Reynolds number. New miniature transducers specifically designed to measure unsteady pressures in a cryogenic environment make these measurements possible. The study reported in this paper was conducted in the 0.3-m Transonic Cryogenic Tunnel (0.3-m TCT) at the NASA Langley Research Center.[1] With its combined pressure, cryogenic temperature, and transonic speed capabilities the 0.3-m TCT can provide flight equivalent airfoil results for current aircraft. This tunnel was used in the Advanced Technology Airfoil Test (ATAT) program in extensive steady flow airfoil studies that demonstrated the necessity for high Reynolds number testing.[2] The airfoil used in the present unsteady tests is a fourteen-percent thick, supercritical airfoil, designated Sc(2)-0714, which was developed at the NASA Langey Research Center.[3] The purpose of this test was to obtain unsteady transonic pressure measurements from an oscillating supercritical airfoil over a wide range of Reynolds number to supplement the previous steady flow results. A secondary objective of the test was the development of instrumentation techniques for measuring unsteady pressures at cryogenic temperatures.

The two-dimensional model had a six inch chord and an eight inch span. The test was concentrated at a tunnel freestream Mach number of 0.72, which previous tests indicated to be the design Mach number. Reynolds number (based on a six inch chord) was varied from 6 x 10^6 to 35 x 10^6 and Mach number was varied at two Reynolds numbers. The range of test frequencies was from 5 Hz to 60 Hz at oscillating pitch amplitudes which varied from ±0.25 degrees to ±1.0 degrees. In this paper, selected steady measured data are presented and are compared with GRUMFOIL calculations at Reynolds numbers of 6 x 10^6 and 30 x 10^6. Experimental unsteady results at Reynolds numbers of 6 x 10^6 and 30 x 10^6 are examined for Reynolds number effects. Measured unsteady results at two mean angles of attack at a Reynolds number of 30 x 10^6 are also discussed.

*Senior Research Engineer, Unsteady Aerodynamics Branch, Loads and Aeroelasticity Division, Member AIAA.
**Research Engineer, Unsteady Aerodynamics Branch, Loads and Aeroelasticity Division, Member AIAA.
***Senior Research Engineer, Transonic Aerodynamics Division, National Transonic Facility Operations Branch, Member AIAA.
****Senior Research Engineer, Transonic Aerodynamics Division, Experimental Techniques Branch, Senior Member AIAA.

Apparatus

Model

The Sc(2)-0714 airfoil model is shown in Fig. 1. It was machined from an alloy (Vascomax-200) that has superior dimensional stability properties at cryogenic conditions. A cavity machined in the underside of the wing, Fig. 2, provided the space necessary to mount the transducers. This cavity was closed by a cover plate on which some lower surface transducers were mounted. The wing was supported on one end by a close-fitting tang fixed to a driving plate with machine screws; this end, seen on the left in Fig. 2, was sealed with epoxy. The other end was supported by an integral shaft which rotated in a bushing in the tunnel side wall plate. A sliding seal of felt was used to seal the gap between the end of the oscillating airfoil and the fixed tunnel sidewall plate. The position of the supports was designed to locate the pitch axis at thirty-five percent chord.

Transducers

Forty-three unsteady pressure transducers were mounted internally in the model. Because of space constraints, forty of the transducers were mounted in receptacles connected by a short length (nominally 0.75 inch) of tubing to the orifice. The remaining three transducers were mounted with the transducer head less than 0.1 inch below the surface of the wing. The orifices of these three transducers were paired with tube mounted transducers for comparison purposes. A series of tests was conducted to examine the effects of orifice diameter, tube diameter, and tube length on the dynamic response of the system. At atmospheric conditions there was no significantreduction of dynamic amplitude response or phase shift of the test configuration up to 100 Hz.

The location of the transducers is given schematically in Figures 3(a) and 3(b). The tube-mounted transducer orifices are located alternately in two rows 0.25 inches on either side of the center line. On the top surface the orifice distribution of the twenty-five transducers results in an orifice every 2% of chord to x/c = 0.1 and 4% chord to x/c of 0.70. The distribution of the 15 tube-mounted transducer orifices on the lower surface is 2% to an x/c of 0.1 and increases to 5% thereafter. The close-mounted transducers and reference orifices are located 0.5 inches from the center line.

The elements of the transducer system are shown in Fig. 4. Since the differential pressure between the wing surface and the tunnel static pressure could exceed the rated capability of the transducer, the transducer was referenced to a manifold which in turn was vented to one of five reference orifices. A reference transducer measured the pressure differential between the manifold and the tunnel static pressure.

The final configuration consisted of transducers with a 10 psi range and with outputs of between 5 and 9 mv/psi. Each transducer was mounted in a receptacle which in turn was connected to the 0.015 inch diameter orifice by a 0.75 inch length of .030 inch i.d. tubing.

The connection between the manifold and the reference orifice was interrupted by a porous flow restricter which damped out the oscillating pressure from the static reference orifice (replacing the long lengths of tubing usually used for this purpose). The results of a series of calibrations made on different combinations of porous flow restrictors and tube lengths are given in Fig. 5. The flow restrictors tested were commercially available sintered filters composed of constant diameter particles, with diameters ranging from 10μ to 25μ. Except for the results for two 25μ restrictors in series (shown in the curve labeled l=.5, 2-25μ) the data shown in Fig. 5 are for single flow restrictors. The reduction in unsteady pressures is shown (Fig. 5) as the ratio of the imposed oscillating input pressure amplitude, P_1, to the output pressure amplitude, P_2, as a function of frequency and for different combinations of filters and tube length, l. Also given in the same figure is the time required, t, for the system to reach equilibrium after the application of a static pulse.

Two 25μ filters in series were selected for the wind tunnel test. Because of lack of space in the model the manifolds and flow restricters were located outside the model during the test and were connected to the model with approximately 6 inches of tubing.

The transducers were to be recovered after the test and consequently could not be permanently bonded to the receptacle. A series of tests were conducted with candidate mastics and dummy transducers at 120 deg. K and 20 psi pressure differential to determine which, if any, would maintain a seal after repeated cycling. A mastic supplied by the transducer vendor was selected for the installation.

Drive System

The large variations in temperature (120 deg. K to 320 deg. K) and stagnation pressure (1.4 atm. - 6 atm.) over the operating range of the 0.3M-TCT result in sidewall deformations that required special considerations in the design of the oscillating drive system. Figure 6 shows the model and the drive system installation in the test section. The test section is shown to the right with the test section ceiling removed and can be identified by the two slots on the floor which run under the model. The model is between the test section sidewalls which in turn are between the tunnel plenum spaces and finally, the tunnel pressure-shell or plenum walls. The critical elements of the system are identified in the schematic drawing in Fig. 7. The hydraulic-rotary actuator required the maintenance of precise alignment for the duration of the test. Since the 0.3-m TCT test section floats on a cable suspension system to accommodate thermal contraction at the cold operating conditions,

the actuator and supporting structure were also supported by a system of cables, blocks, and counter weights so that they could move with the test section.

An insulating spacer between the actuator and the drive shaft and two hot air blowers were used to reduce the chill on the actuator and system components external to the tunnel. A Teflon (reg. trade mark) bushing and pressure seal were the remaining fixed support points for the hollow aluminum drive shaft. The shaft was attached to the rotating sidewall drive disk through a bellows that isolated the shaft from the relative in-line movement of the tunnel sidewall. The rotating drive disk was Teflon coated on its circumferential bearing surfaces and had a rectangular slot to accommodate the wing tang. The tang was hollow to provide a path for transducer cables and tubing which went through a matching hole in the plate and exited through the cable ports in the drive shaft. This end of the wing was sealed with epoxy and bolted to the rotating disk.

The other end of the wing was supported by the integral hollow wing shaft and a bushing in the sidewall plate. This end of the wing moved relative to its mounting plate and was sealed with felt that matched the profile of the wing. The wing shaft was attached to a rotary transducer by an insulating shaft. The hollow wing shaft provided a path for the remaining instrumentation cables. The rotary transducer was heated with surface heaters under thermostat control and the entire assembly covered with an insulated can.

The system did not develop any problems during the test. The angle of attack was checked visually against a sidewall scribe mark at the beginning of each days test before the introduction of cryogenic nitrogen caused extensive frost to be formed on the view ports. The correlation of the geometric flow angle of attack between the scribe mark at the trailing edge and the instrumentation did not vary during the test.

Data Acquisition and Reduction

Static data from the model and tunnel instrumentation were acquired using the 0.3M-TCT data acquisition system. The model angle of attack and pressure data were fed to the system's analog data acquisition channels. The system has 192 channels which are filtered with a 10-Hz low-pass filter and then digitized at 20 samples per second. Static data values are acquired by averaging the digitized values over a one second interval.

Dynamic model data were acquired using analog tape recorders. The instrumentation signal was amplified to be a value of about one volt RMS. The model angle of attack and pressures were taken directly from the amplifiers and recorded on two 28-channel analog tapes operating at 15 inches per second. To obtain amplitude and phase information at the frequency of oscillation and the lowest harmonics, the data was digitized at 32 samples per cycle of oscillatory motion for 64 contiguous cycles. A Fast Fourier Transformation average (FFT) was taken of the data to calculate the harmonic components of the unsteady pressures. The data sample rate and number of cycles analyzed was selected to give an accurate estimate of the first three fundamental harmonic componets. The harmonic pressure coefficients are normalized by the amplitude of the harmonic wing motion in degrees. All phase angles were relative to the wing position.

Sidewall boundary layer and angle of attack corrections were applied to the measured steady pressure results. The sidewall boundary layer corrections are based on the theory of Ref. 4 which is used in Ref. 5 with measured values of sidewall displacement and momentum thickness to compile the tables which were used to correct the experimental values in this paper. The angle of attack corrections described in Ref. 6 (sometimes referred to as the "Barnwell-Davis-Moore" correction) adjust the theory of Davis-Moore with experimental data. The wall induced downwash immediately over the model for the 0.3-m TCT is:

$$\Delta\bar{\alpha} = \frac{-C_l c}{8\,(1+j)h}$$

The parameters necessary to make the correction are:

c = chord = 6 in.
h = tunnel semi-height = 12 in.
a = slot spacing = 4 in.
δ = width of slot = 0.2 in.

$j = aK/h$
K = 3.2 (semi empirical constant, function of δ and a)

For $C_l = 1.0$

$\Delta\bar{\alpha} = -1.73245$ deg.

Results and Discussion

The test was designed to explore the effects of Reynolds number on unsteady pressures and to generate a data base for validating unsteady-aerodynamic computer codes. The test conditions as defined by Mach number and Reynolds number are shown in Fig. 8. Test points were taken at the design Mach number of 0.72 at test Reynolds numbers varying from 6 x 10^6 to 30 x 10^6. Mach number was varied at two Reynolds numbers, 15 x 10^6 and 30 x 10^6. A total of 976 test points were taken. The primary data base was taken for pitch-oscillation frequency between 5 Hz and 40 Hz at amplitude of ±0.25 degree as indicated by the open and closed symbols. Once this data was in hand, the pitch amplitude was increased to ±0.5 and ±1.0 degree and the pitch frequency was also increased to 60 Hz at test conditions indicated by the solid symbols.

Steady Pressures

Steady pressure distributions for four angles of attack, $\bar{\alpha}_t$, approximately 2.5°, 2.0°, 1.5°, and 0°, and for two Reynolds

numbers, 6 x 10^6 and 30 x 10^6, are shown in Fig. 9. The experimental data are shown as symbols and the calculations as solid lines. The pressure data have been corrected for sidewall effects (refs. 4 and 5) and angle of attack (ref. 6). Calculated pressure distributions from the full potential GRUMFOIL computer code (ref. 7) are also compared (Fig. 9). The GRUMFOIL code consists of a full potential equation flow solver integrated with a viscous boundary layer model. GRUMFOIL may be entered by specifying either $\bar{\alpha}$ or C_l. The corrected values of Mach number and C_l were used as the input data for the computed results which are compared with the corrected experimental values of C_p shown in Fig. 9. Below each figure are listed M, $\bar{\alpha}$, and C_l values for the tunnel test conditions, the corrected values, and the values resulting from the GRUMFOIL calculations.

The comparisons between experiment, shown as symbols, and calculations, solid lines, in Fig. 9 are very good. The shock moves aft by approximately 8% to 10% of chord for a given value of $\bar{\alpha}_t$ when Reynolds number is increased from 6 x 10^6 to 30 x 10^6. The GRUMFOIL code under-predicts the position of the shock at both Reynolds numbers by approximately 2-3% of chord even though C_l is matched.

Lift coefficients for several cases are shown in Fig. 10 plotted against corrected angle of attack and against angle of attack as computed by GRUMFOIL for input values of Mach number and C_l for Reynolds number of 6 x 10^6 and 30 x 10^6. The angles calculated from GRUMFOIL are consistently larger than those determined from the correction procedure of ref. 6. This trend is similar to the one shown in ref. 8. Irrespective of the angle of attack corrections, an increase in C_l of approximately 0.1 is shown as Reynolds number is increased from 6 x 10^6 to 30 x 10^6. This increase results from the rearward movement of the shock shown in Fig. 9.

Unsteady Pressures

The effects of Reynolds number and frequency of oscillation upon the unsteady pressure distribution is shown in Fig. 11. Results are given in terms of the modulus of the unsteady pressure coefficient normalized by the oscillating pitch angle, α, and the phase angle, ϕ, between the unsteady pressure and the oscillating wing position. Results are shown for $\bar{\alpha}_t$ = 1° and 2° and for R = 6 x 10^6 and 30 x 10^6. Two oscillation frequencies, 5 Hz and 20 Hz, are presented for a pitch amplitude of ±0.25 degrees. The upper surface pressure distributions are shown in Fig. 11(a) and the corresponding lower surface pressures are in Fig. 11(b).

The shock wave, identified by the peak in the unsteady pressures, moves aft about 8% to 10% chord as R is increased from 6 x 10^6 to 30 x 10^6 at the same tunnel test angles. The unsteady pressures, at both Reynolds numbers, are significantly greater ahead of the shock at $\bar{\alpha}_t$ = 1 degree than at 2 degrees. There is no significant difference in the magnitude of the unsteady pressures due to a change in frequency from 5 Hz to 20 Hz.

For the test conditions shown, the pressures ahead of the shock are approximately 180° out of phase with the wing oscillation. Immediately after the shock wave the phase angle at the pressure abruptly changes from -180° to approximately 0° to be in-phase with the wing pitching motions. Aft of the shock wave the phase angle remains at 0° at $\bar{\alpha}_t$ = 2°, but is more dependent on frequency at the lower mean pitch angle, $\bar{\alpha}_t$ = 1°, tending to go back to -180° at 20 Hz and to 0° at 5 Hz.

The lower surface pressures and phase angles are shown in Fig. 11(b). The pressures are low and decrease from leading to trailing edge; the phase angle is close to zero except at the region of the lower surface inflection.

The effect of varying the amplitude of the pitch oscillation at M = 0.72 is shown in Fig. 12. Pressure distributions are shown for R = 30 x 10^6 for two mean angles, $\bar{\alpha}_t$ = 1° and 2° and for two frequencies, f = 40 and 60 Hz. Data for pitch amplitudes of 0.25, 0.5, and 1.0 degree are shown. In most cases, in this and the following figure, the data points are not connected in the neighborhood of the peak shock amplitude because the peak pressure is not defined by a finite number of pressure orifices. The upper surface pressure distribution, Fig. 12(a), shows a reduction and broadening of the shock-generated peak amplitude as the pitch amplitude, α, is increased from 0.25° to 1° at both frequencies and mean angles. Note the substantial change in mean shock position due to pitch amplitude at f = 60 Hz and $\bar{\alpha}_t$ = 1°.

A secondary peak in the magnitude of the oscillating pressure is evident immediately behind the shock at $\bar{\alpha}_t$ = 2° and 1° which could be attributed to flow separation and reattachment as discussed in Ref. 9. However, an inviscid calculation using the XTRAN2L[10,11] computer code predicts this secondary response, albeit not precisely at the same chord location. Calculations with GRUMFOIL shown in Fig. 13 illustrates that a more probable reason for the secondary response derives from the supersonic regions above the airfoil. At $\bar{\alpha}_t$ = 1° there is a secondary supersonic region behind the shock which is engulfed by the primary supersonic region when the angle of attack is increased to $\bar{\alpha}_t$ = 2°. Tijdeman[12] and others have noted that the flow in the supersonic region prior to the formation of a shock is characterized by a substantial increase in unsteady pressure.

The upper surface phase angle, ϕ, shows changes in the neighborhood of the shock and aft portion of the airfoil with pitch amplitude, Fig. 12(a).

The lower surface pressure amplitude and phase, ϕ, are given in Figure 12(b). Both are

relatively independent of pitch amplitude except in the neighborhood of the inflection or cusp region of the airfoil. Both pressure and phase decrease from leading edge to trailing edge.

The effect of varying the oscillation frequency at M = 0.72 is shown in Fig. 14. Pressure distributions are shown for R = 30 x 10^6 for mean angles $\bar{\alpha}_t$ = 1° and 2° and for pitch amplitudes of 0.25° and 0.5°. Data for frequencies of 5, 15, 40, and 60 Hz are presented. In general the excursion of the shock on the upper surface, Fig. 14(a), is reduced at 60 Hz and again the second peak is greater at $\bar{\alpha}_t$ = 1° than at $\bar{\alpha}_t$ = 2° and is not a strong function of frequency. As expected the phase angle is a function of frequency showing similar characteristics as shown in the previous figure decreasing to approximately 0° behind the shock. The lower surface pressures and phase angle, Fig. 14(b) again decrease from a maximum at the leading edge to a minimum at the trailing edge and showing some dependence on frequency.

Boundary Layer State

The unsteady pressure transducers used in this test also enabled measurements to be obtained which are of interest regarding the state of the boundary layer. The time histories of the pressures at five transducer locations taken when the airfoil was locked at fixed angle of attack are shown in Fig. 15. The data shown in this figure are all at a gain of 10 but the transducer sensitivity, given with each trace, has not been applied to put the time histories in engineering units. The time histories taken at two fixed angles of attack ($\bar{\alpha}_t$ = 0° and 2°) at R = 35 x 10^6 are shown in Fig. 15(a) and Fig. 15(b) respectively. The steady pressure distributions are shown at the right of each figure. The solid points on the pressure distribution mark the location (x/c = .14, .28, .46, .62, .75) of the five transducers. In Fig. 15(a) ($\bar{\alpha}_t$ = 0°) the time histories have the characteristics of a turbulent boundary layer. However in Fig. 15(b) ($\bar{\alpha}_t$ = 2°) the pressure is quiescent at x/c of 0.14 and 0.28 in comparison with the transducer responses at $\bar{\alpha}_t$ = 0°. At an x/c of 0.46 the effect of shock movement is observed. At an x/c of 0.62 the shock movement is still observed and turbulence is apparent. At x/c of 0.75 the signal is comparable to that at $\bar{\alpha}_t$ = 0°. The most obvious difference between the conditions at the two angles of attack is the presence of a shock and the slightly more favorable pressure gradient at $\bar{\alpha}_t$ = 2°. The time histories indicate that laminar flow was present at $\bar{\alpha}_t$ = 2° and that transition to turbulence was between an x/c of 0.28 and 0.46 corresponding to transition Reynolds numbers between 9.8 x 10^6 and 16.1 x 10^6. The possibility exists that long runs of laminar flow existed intermittently during the tests.

Conclusions

Steady and unsteady pressures on a 14 percent supercritical airfoil at transonic Mach numbers have been measured at Reynolds numbers from 6 x 10^6 to 35 x 10^6. Instrumentation techniques were developed to measure unsteady pressures in a cryogenic tunnel at flight Reynolds numbers. Experimental steady data, corrected for wall effects, show very good agreement with calculations from a full potential computer code with an interacted boundary layer. The steady and unsteady pressures both show a shock position that is dependent on Reynolds number. For a supercritical pressure distribution at a chord Reynolds number of 35 x 10^6, laminar boundary layer flow was observed over a significant percentage of the airfoil chord.

Acknowledgement

The authors wish to acknowledge the assistance of Clyde Gumbert of the Theoretical Aerodynamics Branch, NASA Langley Research Center, in the GRUMFOIL calculations.

References

[1]Ray, E. J.; Ladson, C. L.; Adcock, J. B.; Lawing, P. L.; and Hall, R. M.: "Review of Design and Operational Characteristics of the 0.3M Transonic Cryogenic Tunnel." NASA TM 80123, 1979.

[2]Ray, E. J.: "A Review of Reynolds Number Studies Conducted in the Langley 0.3M-Transonic Cryogenic Tunnel." AIAA/ASME 3rd Joint Thermophysics, Fluids, Plasma and Heat Transfer Conference, St. Louis, MO, June 7-11, 1982. AIAA Paper 82-0941.

[3]Harris, C. D.: "Aerodynamic Characteristics of a 14-Percent Thick NASA Supercritical Airfoil Designed for a Normal-Force Coefficient of 0.7." NASA TM X-72712, July 1975.

[4]Sewall, W. G.: "The Effects of Sidewall Boundary Layer in Two-Dimensional Subsonic and Transonic Wind Tunnels." AIAA Journal, Vol. 20, No. 9, September 1982, pp. 1253-1256.

[5]Jenkins, R. V.; and Adock, J. B.: "Tables for Correcting Airfoil Data Obtained in the Langley 0.3-Meter Transonic Cryogenic Tunnel for Sidewall Boundary Layer Effects." NASA TM 87723, June 1986.

[6]Barnwell, R. W.: "Design and Performance Evaluation of Slotted Walls for Two-Dimensional Wind Tunnels." NASA TM 78648, February 1978.

[7]Mead, H. R.; and Melnik, R. E.: "GRUMFOIL: A Computer Code for the Viscous Transnic Flow Over Airfoils." NASA CR 3806, October 1985.

[8]Gumbert, C. R.; and Newman, P. A.: "Validation of a Wall Interference Assessment/Correction Procedure for Airfoil Tests in the 0.3M-Transonic Cryogenic Tunnel." AIAA 2nd Applied Aerodynamics Conference, August 21-23, 1984.

[9]Mundell, A. R. G.; and Mabey, D. G.: "Pressure Fluctuations Caused by Transonic Shock/Boundary-Layer Interaction." Aeronautical Journal, August/September 1986.

[10]Whitlow, W., Jr.: "XTRAN2L: A Program for Solving the General Frequency Unsteady Transonic Small Disturbance Equation," NASA TM 85721, November 1983.

[11]Seidel, D. A.; and Batina, J. T.: "User's Manual for XTRAN2L (Version 1.2): A Program for Solving the General-Frequency Unsteady Transonic Small-Disturbance Equation," NASA TM 87737, July 1986.

[12]Tijdeman, H.: "Investigation of the Transonic Flow Around Oscillating Airfoils," NLR TR 77090 U, 1977.

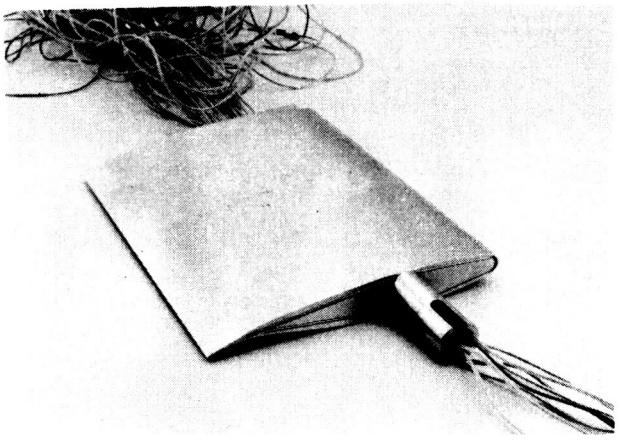

Fig. 1 External view of model.

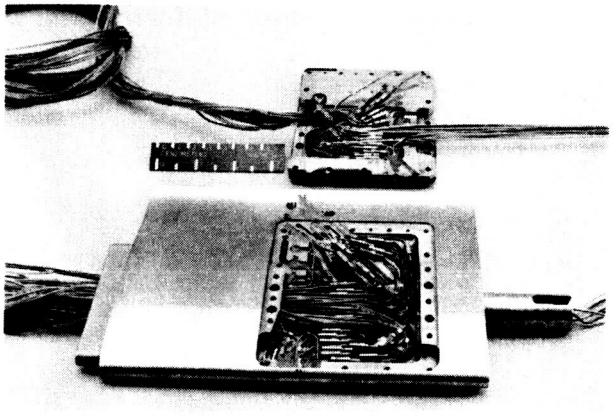

Fig. 2 Internal configuration of model.

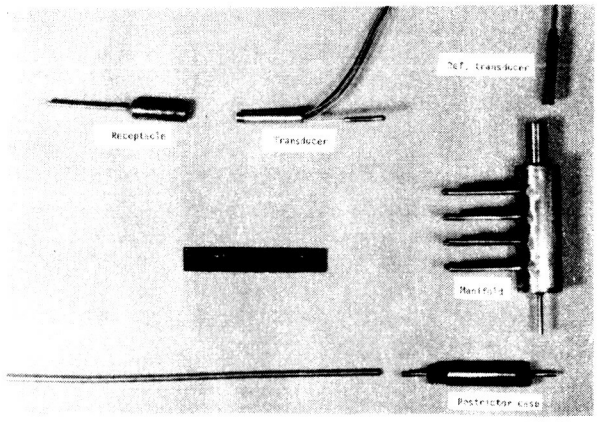

Fig. 4 Elements of the transducer system.

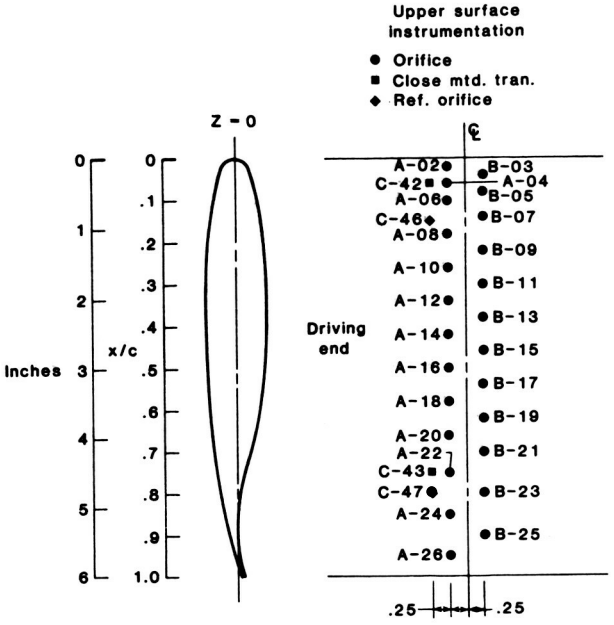

(a) Upper surface

Fig. 3a Transducer locations.

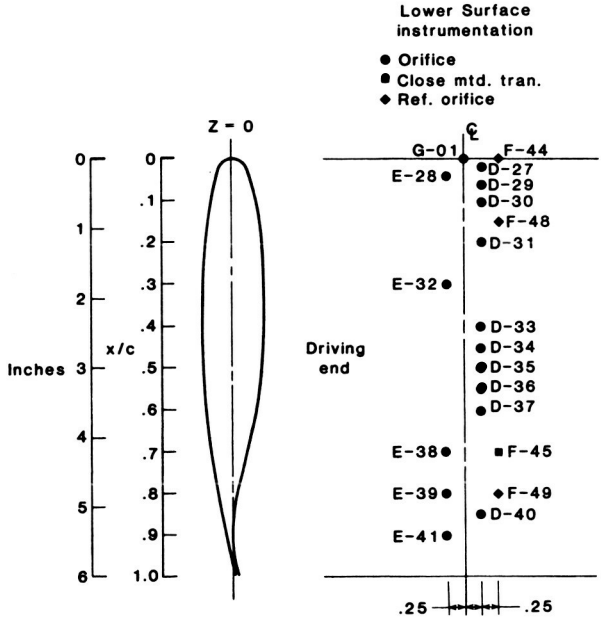

(b) Lower surface

Fig. 3b concluded.

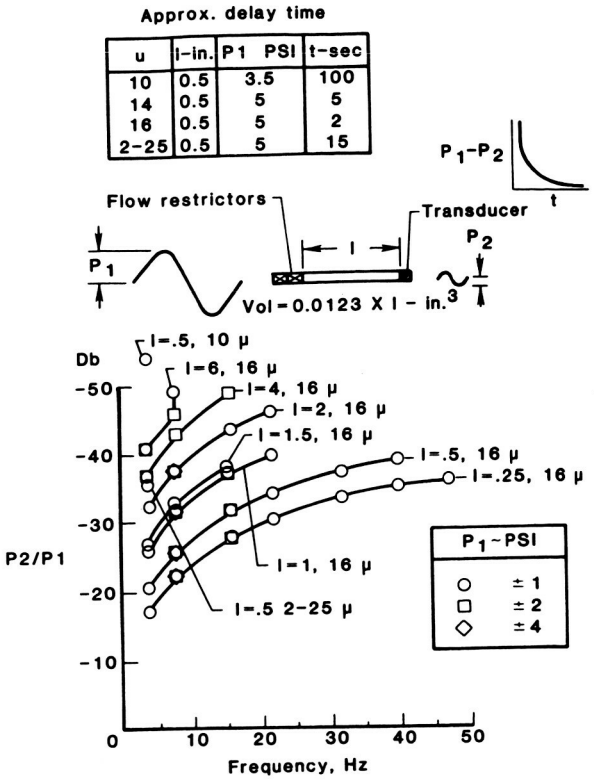

Fig. 5 Dynamic flow-restrictor-tube calibration results.

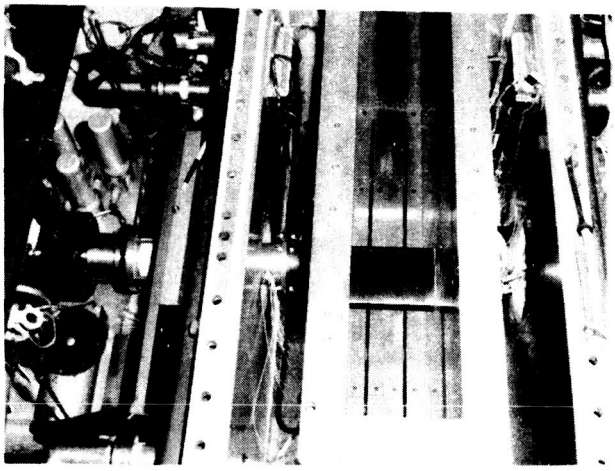

Fig. 6 Model installation.

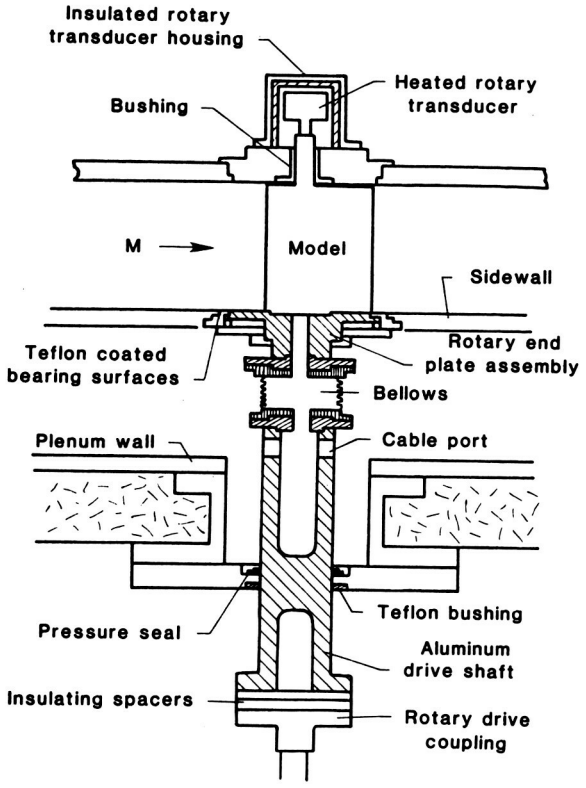

Fig. 7 Schematic drawing of model installation.

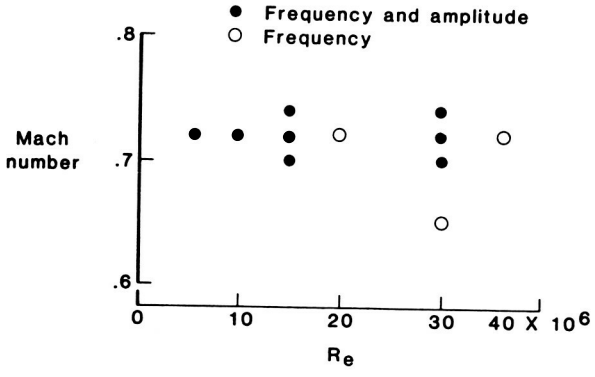

Fig. 8 Mach number and Reynolds number test conditions.

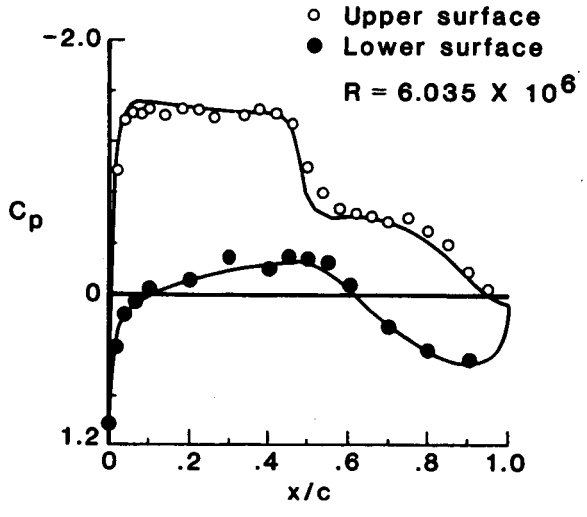

	Tunnel	Corrected	Grumfoil
M	0.720	0.701	0.701
$\bar{\alpha}$	2.504	0.844	1.385
C_l	0.9581	0.9753	0.9837

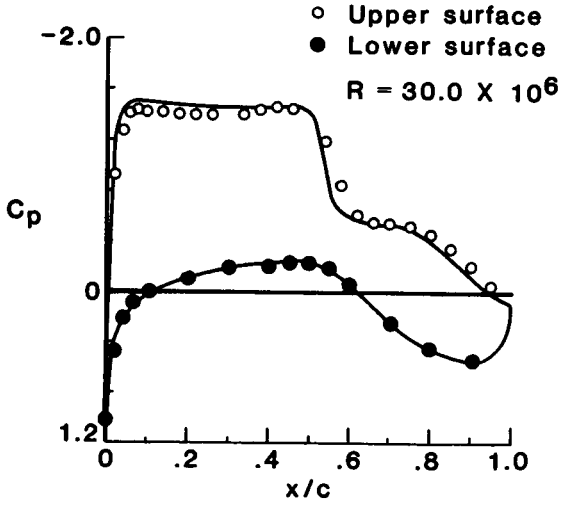

	Tunnel	Corrected	Grumfoil
M	0.719	0.705	0.705
$\bar{\alpha}$	2.51	0.756	1.399
C_l	1.0123	1.0256	1.0336

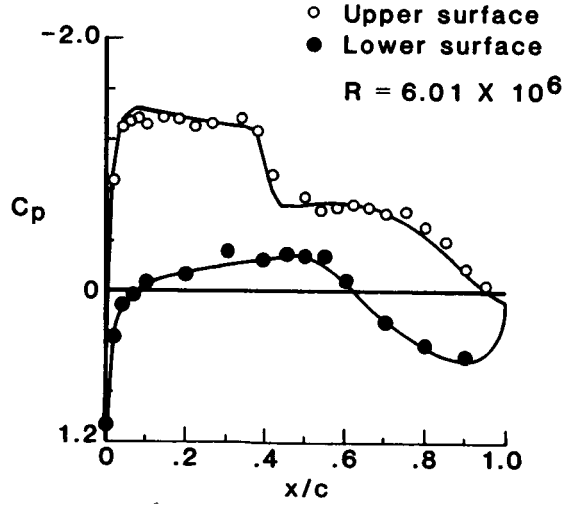

	Tunnel	Corrected	Grumfoil
M	0.72	0.701	0.701
$\bar{\alpha}$	2.002	0.525	0.961
C_l	0.8523	0.8676	0.8757

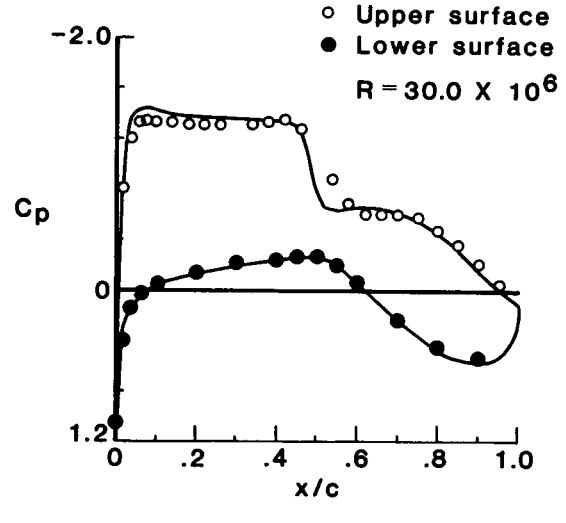

	Tunnel	Corrected	Grumfoil
M	0.721	0.705	0.705
$\bar{\alpha}$	1.997	0.393	0.910
C_l	0.926	0.939	0.9453

Fig. 9 Comparisons of steady test results with calculated results at a tunnel Mach number of 0.72.

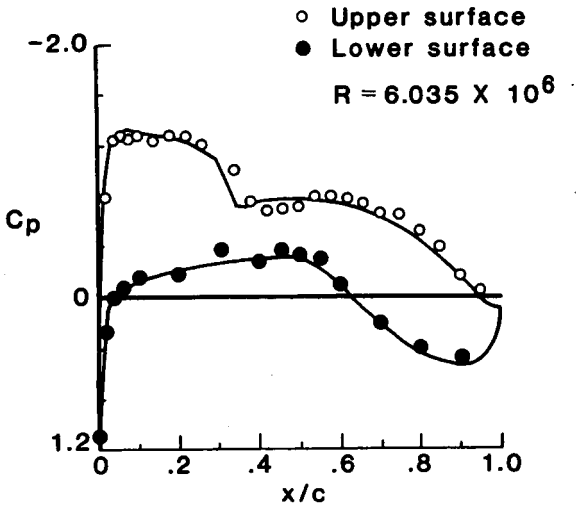

	Tunnel	Corrected	Grumfoil
M	0.719	0.701	0.701
$\bar{\alpha}$	1.495	0.201	0.493
C_l	0.7467	0.7601	0.7680

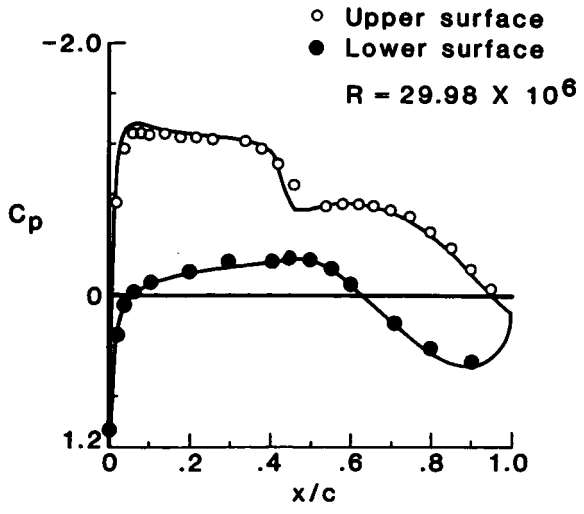

	Tunnel	Corrected	Grumfoil
M	0.718	0.705	0.705
$\bar{\alpha}$	1.501	0.051	0.552
C_l	.8373	0.849	0.8555

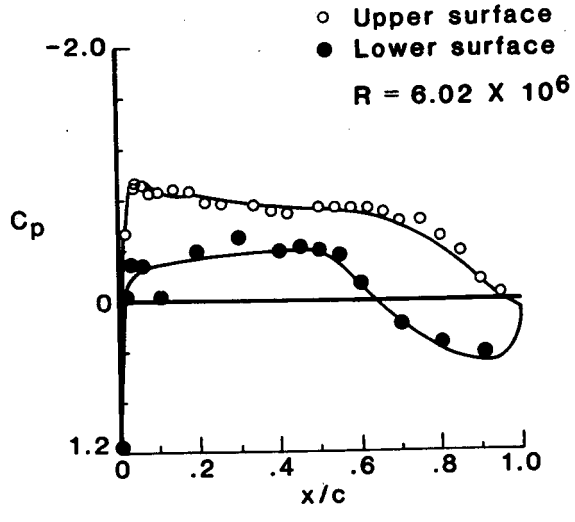

	Tunnel	Corrected	Grumfoil
M	0.720	0.701	0.701
$\bar{\alpha}$	0.004	-0.92	-0.398
C_l	0.5288	0.5383	0.5484

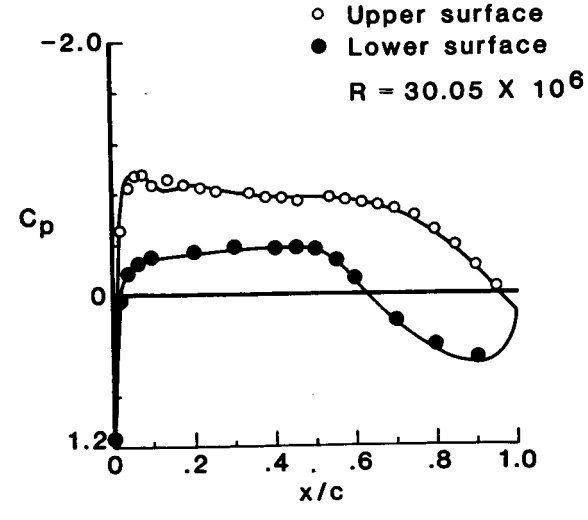

	Tunnel	Corrected	Grumfoil
M	.721	0.705	0.705
$\bar{\alpha}$	-0.005	-1.036	-0.715
C_l	0.5951	0.6034	0.6099

Fig. 9 concluded.

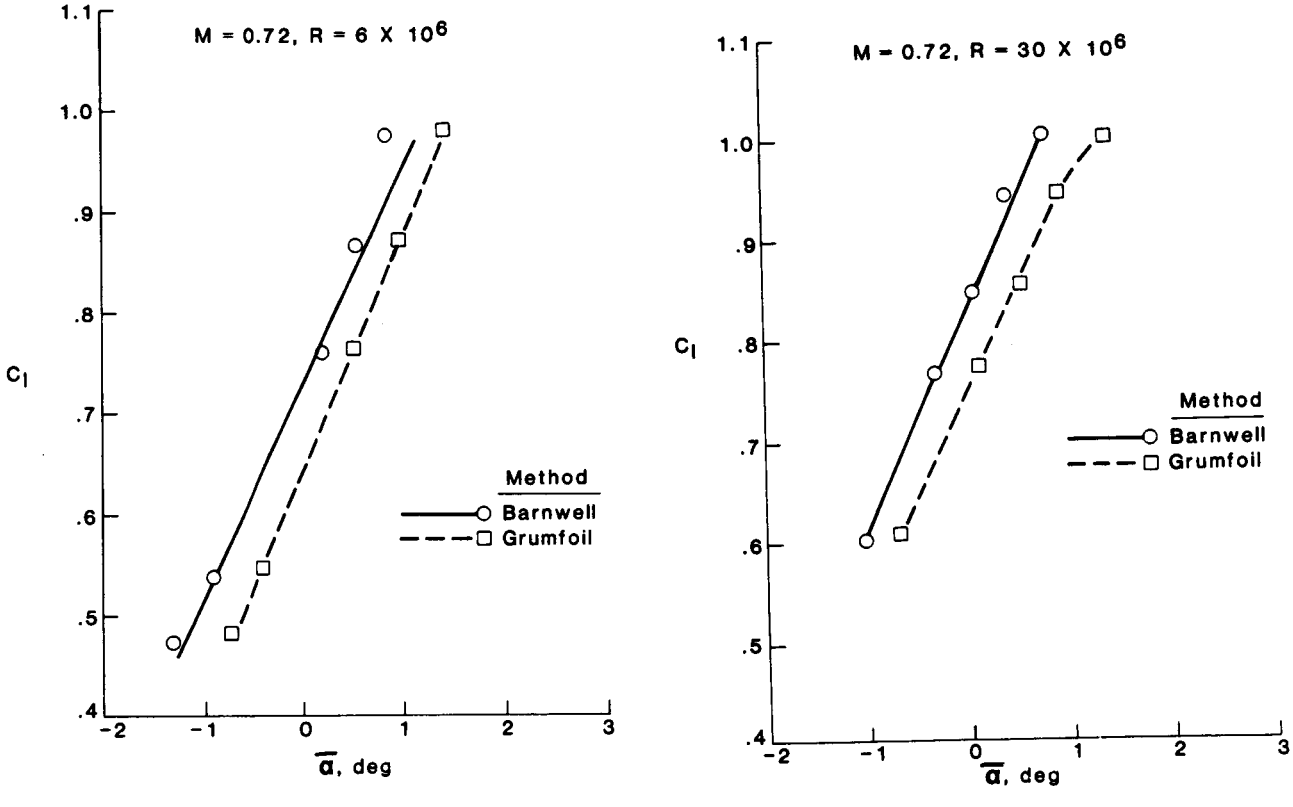

Fig. 10 Comparison of lift coefficient versus corrected angle-of-attack.

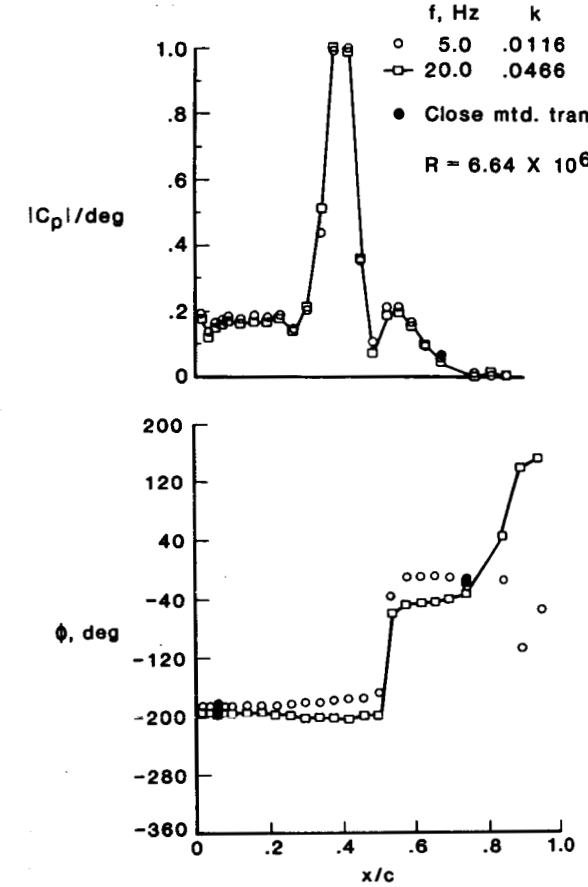

$\bar{\alpha}_t$ = 2.06°, $\bar{\alpha}_c$ = 0.59°.

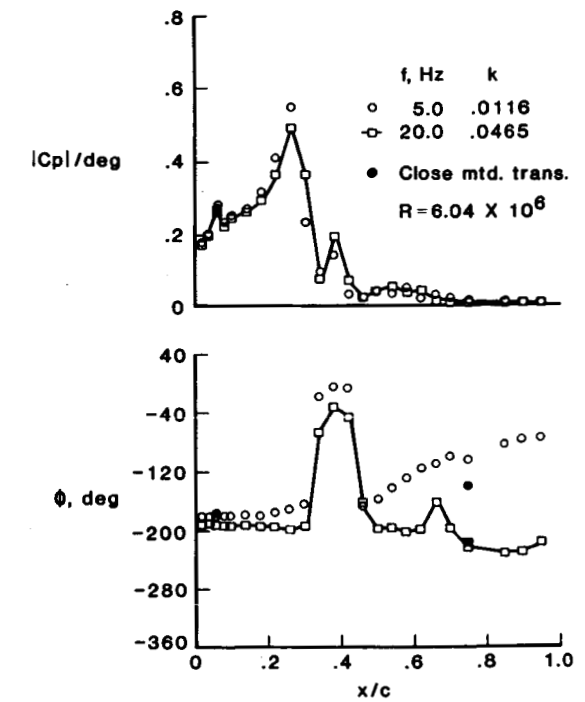

$\bar{\alpha}_t$ = 1.036°, $\bar{\alpha}_c$ = -0.561°

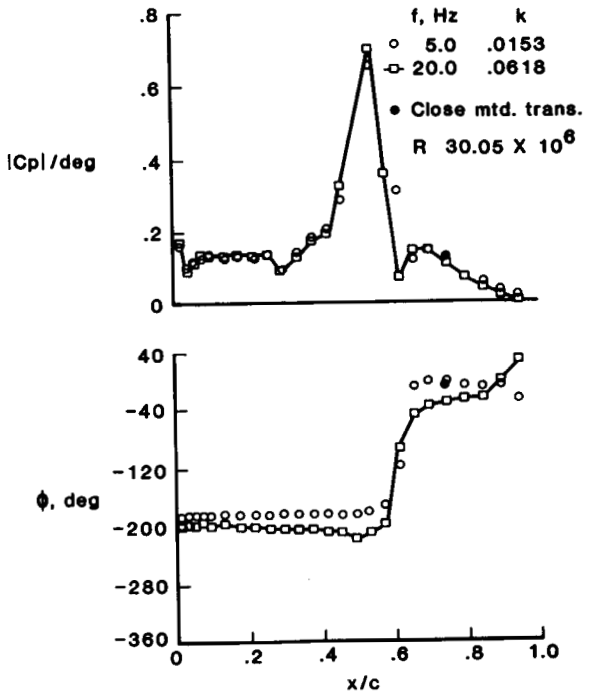

$\bar{\alpha}_t$ = 2.05°, $\bar{\alpha}_c$ = 0.446°

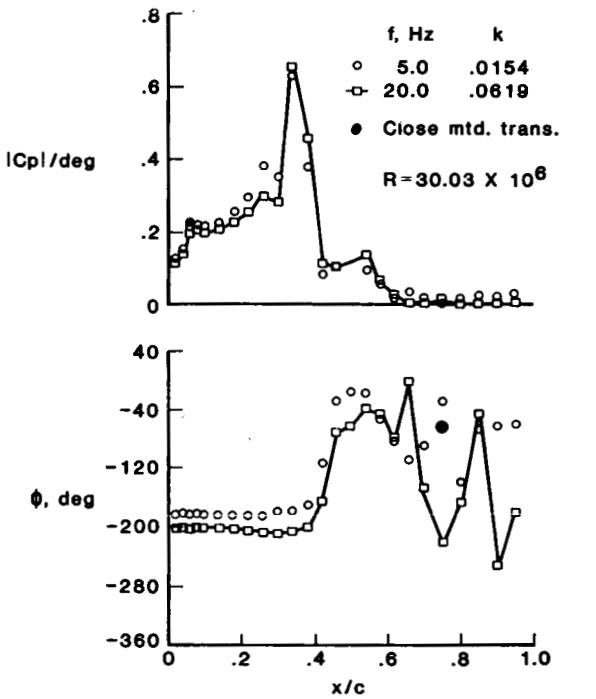

$\bar{\alpha}_t$ = 1.05°, $\bar{\alpha}_c$ = -0.255°

(a) Upper surface

Fig. 11 Unsteady pressure test results at a tunnel Mach number of 0.72 and at α = ±0.25°.

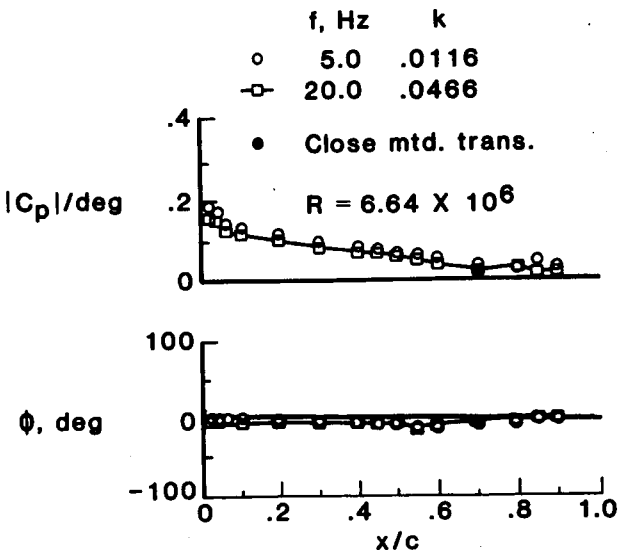

$\bar{\alpha}_t = 2.06°$, $\bar{\alpha}_c = 0.59°$

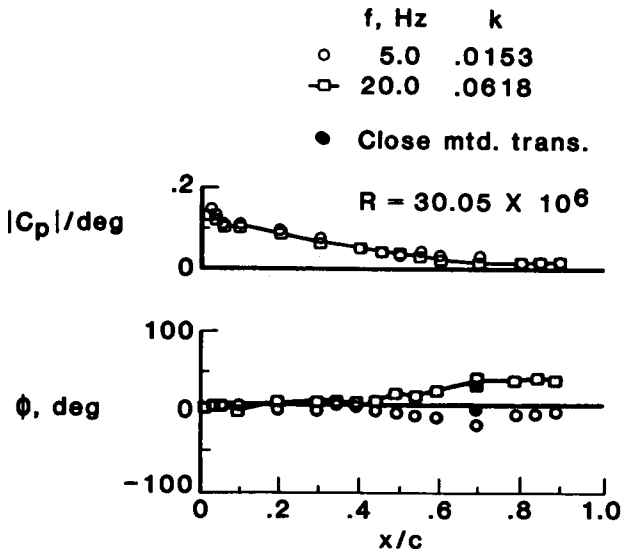

$\bar{\alpha}_t = 2.05°$, $\bar{\alpha}_c = 0.446°$

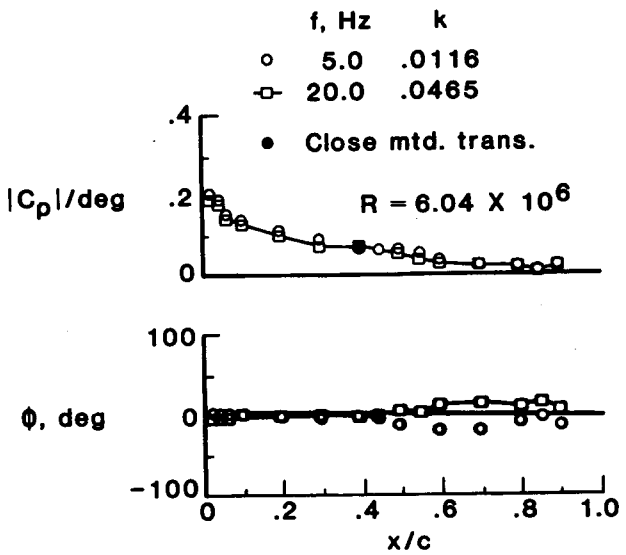

$\bar{\alpha}_t = 1.036°$, $\bar{\alpha}_c = -0.561°$

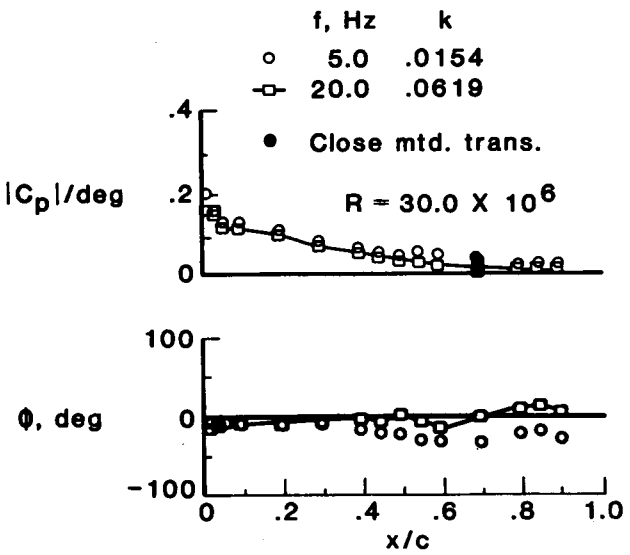

$\bar{\alpha}_t = 1.05°$, $\bar{\alpha}_c = -0.255°$

(b) Lower surface

Fig. 11 concluded.

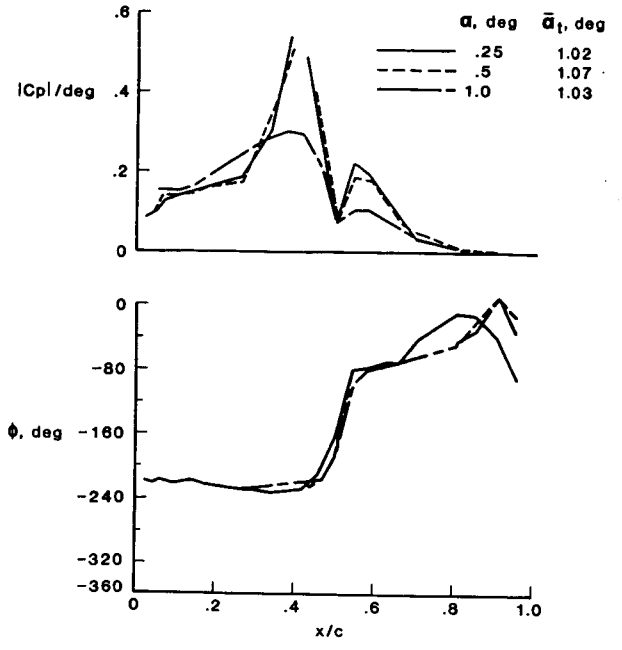

f = 40 Hz

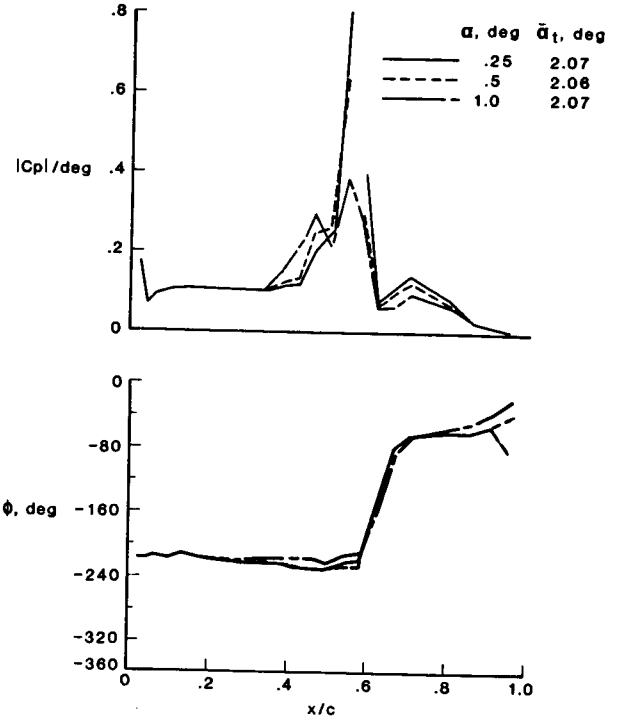

f = 40 Hz

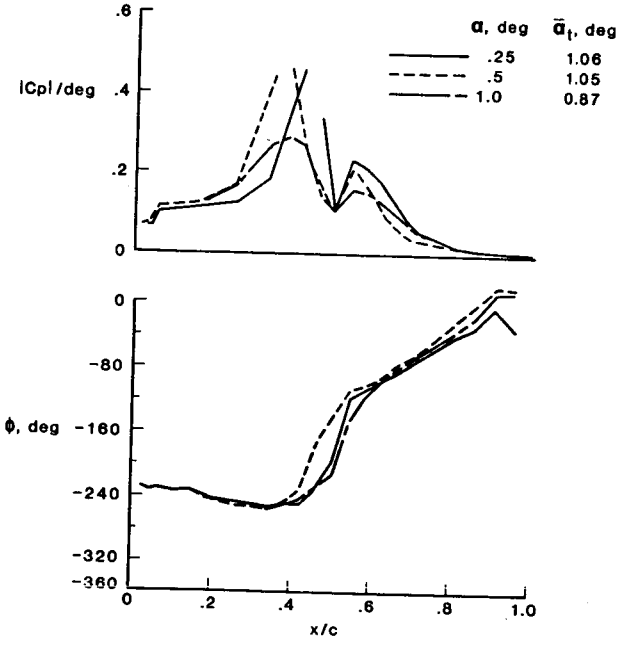

f = 60 Hz

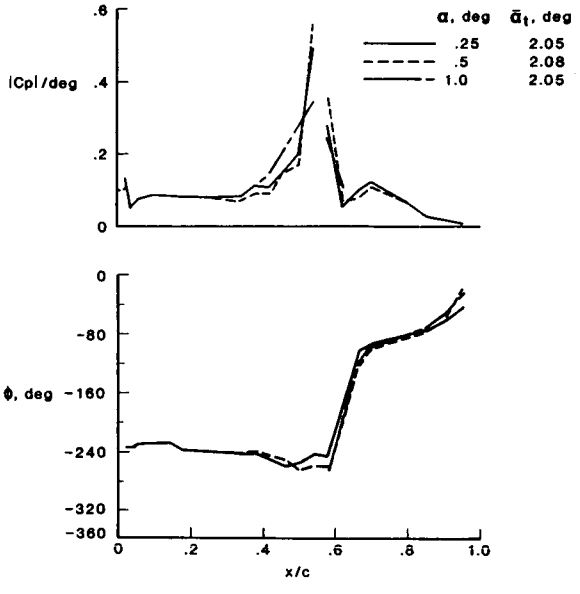

f = 60 Hz

Fig. 12 Variation of $|C_p|$/deg and ϕ at M = 0.72 and R = 30 x 10^6 with pitch amplitude.

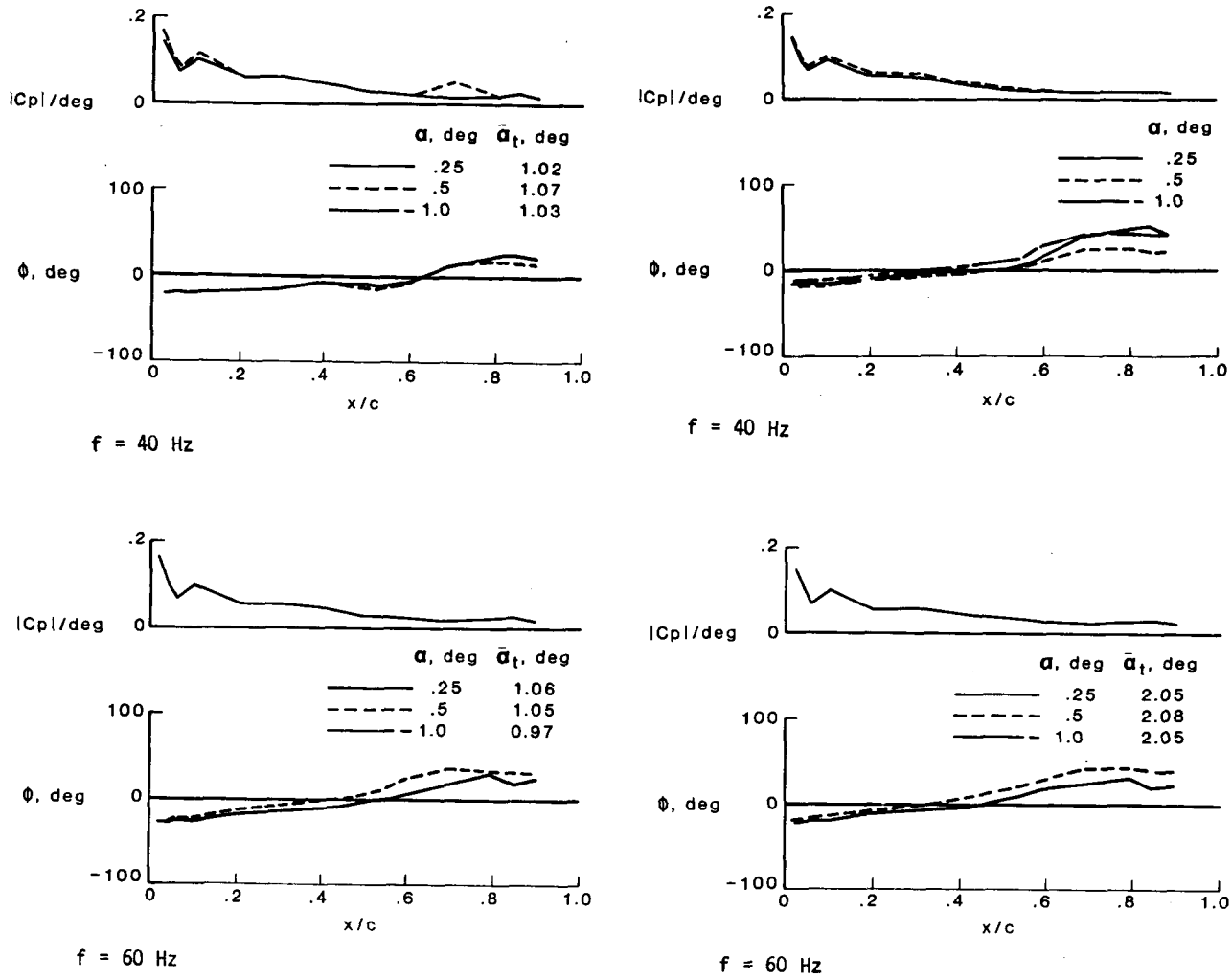

(b) Lower surface

Fig. 12 concluded.

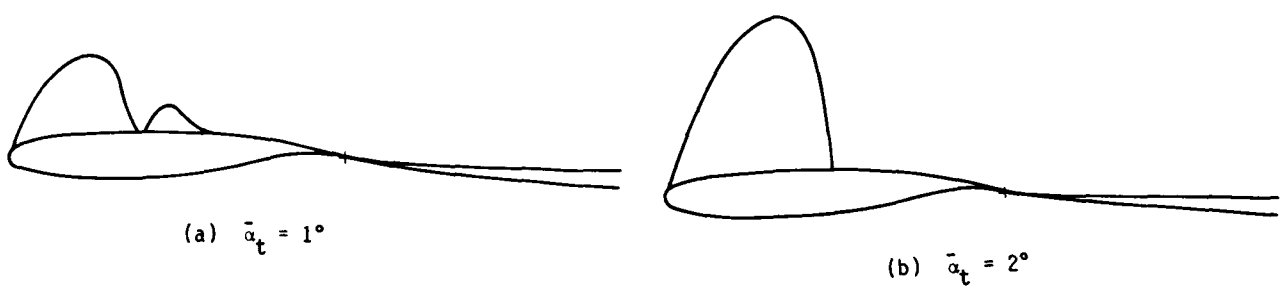

(a) $\bar{\alpha}_t = 1°$

(b) $\bar{\alpha}_t = 2°$

Fig. 13 Sonic regions at M = 0.72 calculated by GRUMFOIL code.

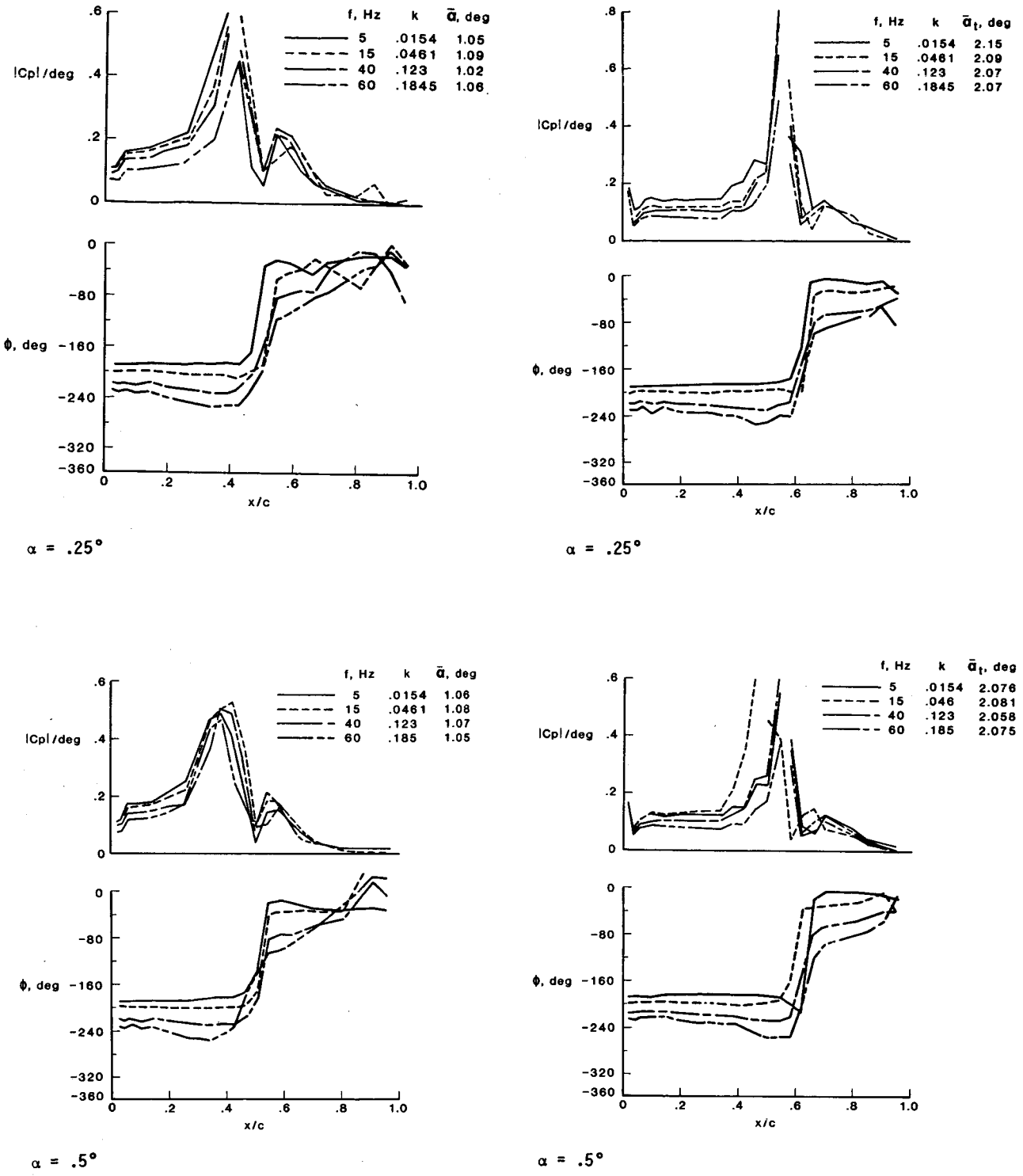

(a) Upper surface

Fig. 14 Variation of $|C_p|$/deg and ϕ at M = 0.72 and R = 30 x 10^6 with frequency

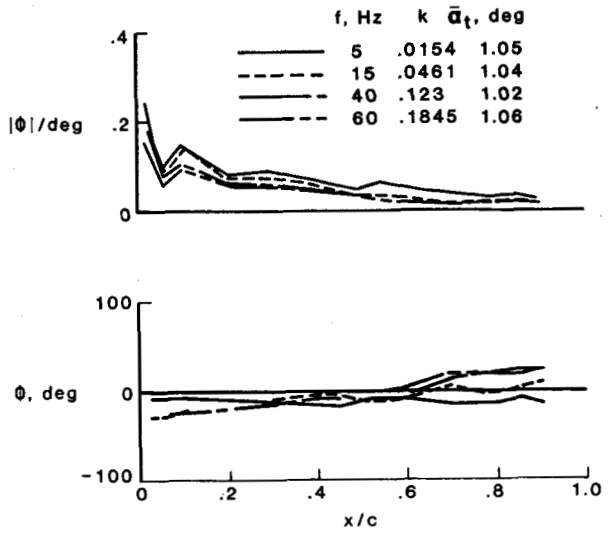

α = .25°

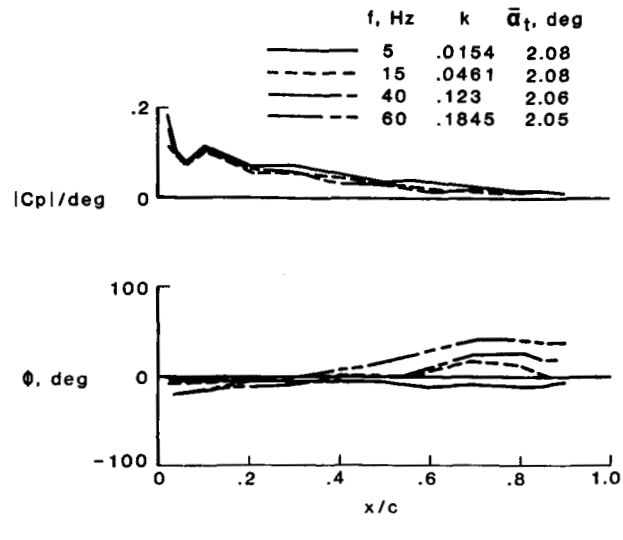

α = .25°

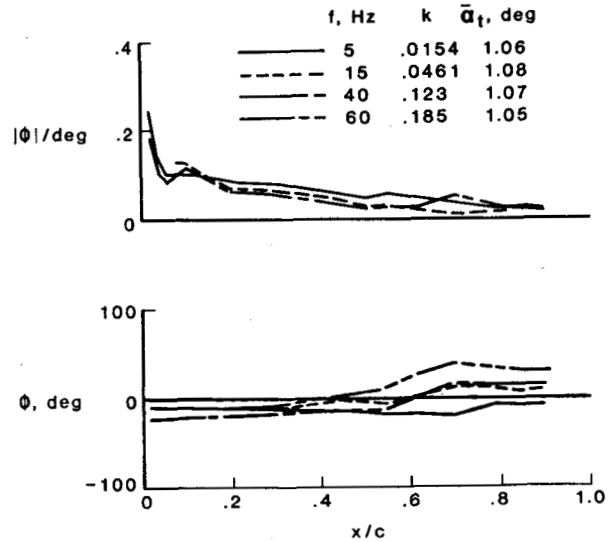

α = .5°

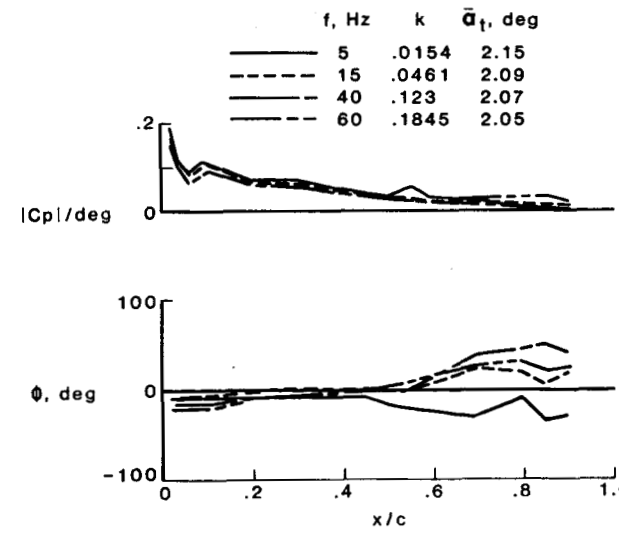

α = .5°

(b) Lower surface

Fig. 14 concluded.

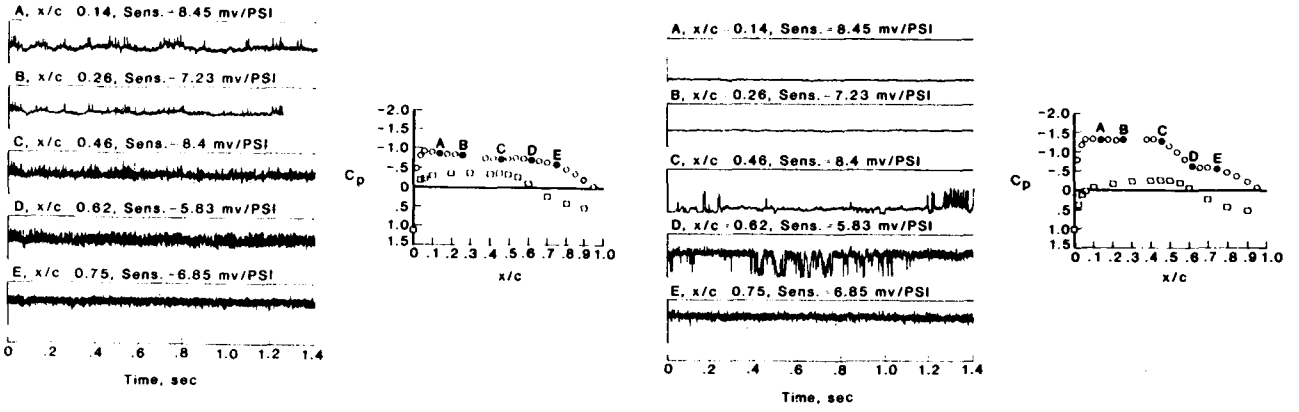

(a) $\bar{\alpha}_t = 0°$.

(b) $\bar{\alpha}_t = 2°$.

Fig. 15 Time histories at five chord stations for $\alpha = 0$, $M = 0.72$, and $R = 35 \times 10^6$.

Standard Bibliographic Page

1. Report No.	2. Government Accession No.	3. Recipient's Catalog No.
NASA TM-89080, Corrected Copy		

4. Title and Subtitle	5. Report Date
Highlights of Unsteady Pressure Tests on a 14 Percent Supercritical Airfoil at High Reynolds Number, Transonic Condition	January 1987
	6. Performing Organization Code: 505-63-21-01
7. Author(s): Robert W. Hess, David A. Seidel, William B. Igoe, and Pierce L. Lawing	8. Performing Organization Report No.
9. Performing Organization Name and Address: NASA Langley Research Center, Hampton, Virginia 23665-5225	10. Work Unit No.
	11. Contract or Grant No.
12. Sponsoring Agency Name and Address: National Aeronautics and Space Administration, Washington, DC 20546	13. Type of Report and Period Covered: Technical Memorandum
	14. Sponsoring Agency Code

15. Supplementary Notes
This paper will be presented at the AIAA 25th Aerospace Sciences Meeting, Reno, Nevada, January 12-15, 1987, as AIAA Paper No. 87-0035.

16. Abstract

Steady and unsteady pressures were measured on a 2-D supercritical airfoil in the Langley Research Center 0.3-m Transonic Cryogenic Tunnel at Reynolds numbers from 6×10^6 to 35×10^6. The airfoil was oscillated in pitch at amplitudes from ±.25 degrees to ±1.0 degrees at frequencies from 5 Hz to 60 Hz. The special requirements of testing an unsteady pressure model in a pressurized cryogenic tunnel are discussed. Selected steady measured data are presented and are compared with GRUMFOIL calculations at Reynolds number of 6×10^6 and 30×10^6. Experimental unsteady results at Reynolds numbers of 6×10^6 and 30×10^6 are examined for Reynolds number effects. Measured unsteady results at two mean angles of attack at a Reynolds number of 30×10^6 are also examined.

17. Key Words (Suggested by Authors(s))	18. Distribution Statement
Reynolds number Steady and Unsteady Pressure Supercritical Wing Mach Number	Unclassified - Unlimited Subject Category - 02

19. Security Classif.(of this report)	20. Security Classif.(of this page)	21. No. of Pages	22. Price
Unclassified	Unclassified	18	A05

For sale by the National Technical Information Service, Springfield, Virginia 22161